Monthly Notices
of the
ROYAL ASTRONOMICAL SOCIETY

MNRAS **462,** 1101–1110 (2016)
Advance Access publication 2016 July 19

doi:10.1093/mnras/stw1717

X-ray and radio emission from the luminous supernova 2005kd

V. V. Dwarkadas,[1]★ C. Romero-Cañizales,[2,3,4]★ R. Reddy[1] and F. E. Bauer[3,2,5]★

[1]*Department of Astronomy and Astrophysics, U Chicago, 5640 S Ellis Ave, Chicago, IL 60637, USA*
[2]*Millennium Institute of Astrophysics, 7500011, Chile*
[3]*Instituto de Astrofísica, Facultad de Física, Pontificia Universidad Católica de Chile, Casilla 306, Santiago 22, Chile*
[4]*Núcleo de Astronomía de la Facultad de Ingeniería, Universidad Diego Portales, Av. Ejército 441, 8370191 Santiago, Chile*
[5]*Space Science Institute, 4750 Walnut Street, Suite 205, Boulder, CO 80301, USA*

Accepted 2016 July 14. Received 2016 July 13; in original form 2015 May 26

ABSTRACT

SN 2005kd is among the most luminous supernovae (SNe) to be discovered at X-ray wavelengths. We have re-analysed all good angular resolution (better than 20 arcsec full width at half-maximum point spread function) archival X-ray data for SN 2005kd. The data reveal an X-ray light curve that decreases as $t^{-1.62\pm0.06}$. Our modelling of the data suggests that the early evolution is dominated by emission from the forward shock in a high-density medium. Emission from the radiative reverse shock is absorbed by the cold dense shell formed behind the reverse shock. Our results suggest a progenitor with a mass-loss rate towards the end of its evolution of $\geq 4.3 \times 10^{-4}$ M$_\odot$ yr^{-1}, for a wind velocity of 10 km s^{-1}, at 4.0×10^{16} cm. This mass-loss rate is too high for most known stars, except perhaps hypergiant stars. A higher wind velocity would lead to a correspondingly higher mass-loss rate. A luminous blue variable star undergoing a giant eruption could potentially fulfill this requirement, but would need a high mass-loss rate lasting for several hundred years, and need to explain the plateau observed in the optical light curve. The latter could perhaps be due to the ejecta expanding in the dense circum-stellar material at relatively small radii. These observations are consistent with the fact that Type IIn SNe appear to expand into high-density and high mass-loss rate environments, and also suggest rapid variability in the wind mass-loss parameters within at least the last 5000 yr of stellar evolution prior to core-collapse.

Key words: circumstellar matter – stars: massive – stars: mass-loss – supernovae: individual: SN 2005kd – stars: winds, outflows – X-rays: individual: SN 2005kd.

1 INTRODUCTION

The core-collapse of a massive star greater than about 8 M$_\odot$ results in a spectacular explosion, and the expansion of a very high-velocity shock wave into the ambient medium, leading to the formation of a supernova (SN) of Type II or Type Ib/c. Type II SNe are further divided into different subclasses, depending mainly on their optical spectra or light curve. Type IIn SNe form one of the more recent subclasses of Type II SNe, having been first identified in 1990 (Schlegel 1990). They are characterized by narrow lines on a broad base in the optical spectrum (Schlegel 1990; Kankare et al. 2012; Mauerhan et al. 2013). Surveys have revealed that they comprise between 1 and 4 per cent of the total core collapse SN population in a volume-limited sample (Eldridge et al. 2013). Observations at optical (Filippenko 1997; Taddia et al. 2013), infrared (Fox et al. 2011), X-ray (Dwarkadas, Dewey & Bauer 2010; Chandra et al. 2012), and radio (Chandra et al. 2009, 2012) suggest that this class of SNe arises from circum-stellar interaction with a high-density medium. Spectropolarimetric observations of luminous IIns (Bauer et al. 2012) are consistent with circum-stellar interaction, but point to a complex origin for the various emission components.

There exists a wide diversity in SNe that exhibit IIn features, which has greatly complicated the task of identifying their progenitors. The prototypical IIns SN 1986J, SN 1988Z, and SN 1978K were only observed years after explosion. More recently, transient surveys have found SNe that show IIn-like features very early in their evolution. Despite over two decades of study, no consensus has been reached on the identity of their progenitor stars, and it seems quite likely that the class of IIns does not have one class of progenitors. Luminous blue variable (LBV) stars have been suggested as the progenitors of IIns (Gal-Yam & Leonard 2009; Smith 2010), although this has been disputed by some authors (Dwarkadas 2011). Analysis of some IIns led Dwarkadas (2011) to suggest that red supergiant (RSG) stars that undergo high mass-loss at the end of their lifetimes could be IIn progenitors, while Smith, Hinkle & Ryde (2009) have suggested extreme RSGs, such as VY

★ E-mail: vikram@oddjob.uchicago.edu (VVD); cristina.romero.fdi@mail.udp.cl (CR-C); fbauer@astro.puc.cl (FEB)

Table 1. Summary of X-ray data on SN 2005kd, listing the satellite which took the observation, the rest-frame-corrected days after explosion, the exposure time, the column density and derived temperatures, and *k*-corrected unabsorbed fluxes, all with 1σ error bars where available.

Satellite	Obs date	Days after outburst[a]	Days after outburst (rest frame)	Exposure (ks)	Count rate (10^{-3} counts s^{-1})	N_H ($10^{22}cm^{-2}$)	kT (keV)	0.3–8 keV flux[b] (10^{-14} erg s^{-1} cm^{-2})
Swift	2007-01-24	440	433.5	8.9	3.9±0.7	0.4±0.27	17±7	26^{+13}_{-11}
Chandra	2007-03-04	479	472.0	3.0	22±2.7	0.77±0.17	>20	$49.6^{+27}_{-16.8}$
XMM[c]	2007-03-29	504	496.5	54.2	15±0.7	0.94±0.29	>30	$41.4^{+4.1}_{-9.4}$
Chandra	2008-01-03	784	772.4	5.0	17±1.8	0.95±0.49	6±0.1	$44.6^{+25.}_{-25.3}$
Swift	2008-08-21	1015	1000.0	9.3	2.2±0.5	0.75[d]	$4.9^{+35}_{-2.3}$	$19.86^{+1.87}_{-6.93}$
Swift	2011-10-22 to 2012-01-05	2200	2167.4	9.9	0.96	0.4[d]	3.5[d]	< 6.7
Swift	2012-06-01 to 2012-07-16	2419	2383.0	16.5	0.7±0.3	$0.15^{e+0.15}_{\text{min}}$	$4.4^{f\,[+75.5]}_{-2.9}$	$3.35^{+0.18}_{-1.65}$
Chandra	2013-11-29	2940	2896.5	29.0	2.4±0.4	$0.43^{+0.12}_{-0.28}$	$3.12^{+30}_{-0.4}$	$1.98^{+0.44}_{-0.36}$

Notes. [a]average value in case of combined exposures,
[b]using cstat statistic (except *XMM–Newton*),
[c]average MOS1, MOS2,
[d]assumed,
[e]converges to minimum set value (Galactic value),
[f]upper bound unconstrained.

CMa as Type IIn progenitors. Thus, although many theories exist, identifying the progenitors will require observations and analysis of a large sample of Type IIns over the entire wavelength spectrum.

SN 2005kd was discovered in an automated search by Puckett & Pelloni (2005) on 2005 November 12.22 UT. It was confirmed by Eastman et al. (2005) to be a Type IIn SN. It lies in the galaxy LEDA 14370, at a redshift of $z = 0.015\,040$, which translates to a luminosity distance of about 63.2 Mpc ($H_0 = 71\,km\,s^{-1}\,Mpc^{-1}$, $\Omega_{matter} = 0.27$, $\Omega_{vacuum} = 0.73$). X-ray and UV emission was observed at the position of the SN with Swift in 2007 January (Immler, Pooley & Brown 2007). Following this, X-ray emission was detected with *Chandra* (Pooley, Immler & Filippenko 2007). The SN was also detected in the radio band at 8.4 GHz (Chandra & Soderberg 2007). This is one of the furthest SNe to be detected in X-rays, suggesting an unusually high X-ray luminosity. SN 2005kd was observed in the infrared by the *WISE* satellite, however, the detection is questionable due to the proximity of the host nucleus (Fox et al. 2013; Fox, private communication).

The optical light curve of SN 2005kd (Tsvetkov 2008) shows an unusually long plateau stage, unique for a Type IIn SN, which lasted for at least 192 d. The UV light curves (Pritchard et al. 2014) show an even larger timespan where the flux appears to be either constant or even increasing. Clearly, even for the strange class of Type IIns, this represents a unique evolution.

In this paper, we re-analyse and present all available X-ray data on SN 2005kd, combined with a 29 ks *Chandra* spectrum that we obtained in 2013 November. We use this data to study the evolution of the X-ray light curve, the nature of the X-ray emission, the density structure of the surrounding medium, and thereby the mass-loss properties of the progenitor star. In Section 2, we summarize the available data, and describe the X-ray data reduction and fitting methods. Section 3 presents the X-ray light curve of SN 2005kd. In Section 4, we interpret the light curve using semi-analytic calculations, use it to extract information regarding the medium which the SN is expanding in, and attempt to delineate the SN progenitor. Motivated by the results from this section, in Section 5, we present available radio archival data that we have reduced and analysed in order to improve our understanding of the SN evolution. Finally, Section 6 summarizes our work, and places this SN in the context of other IIn SNe as well as the complete group of core-collapse SNe.

2 DATA ANALYSIS

SN 2005kd was first detected in the X-ray band around 15 months after explosion, and thus no data exist for the first year of evolution. We have reduced all good angular resolution [<20 arcsec full width at half maximum (FWHM) point spread function (PSF)] data, including data from *Swift*, *Chandra* and *XMM–Newton*. The exposure times in general were short, such that much of the data has low signal to noise. Table 1 summarizes the available data and lists the derived fluxes.

The data from each satellite were reduced according to the standard reduction procedures. X-ray spectral fitting was done using SHERPA with thermal XSPEC models. We have presented results using the *vmekal* models, but note that using either *raymond* or *apec* models does not alter the derived conclusions. Given the low number of data counts in all cases except for the *XMM–Newton* pointing, all fits and flux estimations were done by fitting the background first using a polynomial function, and then simultaneously fitting the data plus the background, using the *cstat* statistic on unbinned data. The high statistics of the *XMM–Newton* observation allowed use of the *chi2gehrels* statistic on binned data combined with background subtraction. The flux estimates are shown in Table 1. Below, we discuss the data reduction and analysis in detail.

2.1 *XMM–Newton*

The SN was observed at an age of 500 d using *XMM–Newton*. This is the longest exposure, with by far the best spectral resolution and effective area, and was used as a template for the subsequent data reduction. The >600 source counts allow for a reliable fitting of the spectrum, providing the model template that we adopted to fit all the other spectra. A 25 arcsec region was used for the source, with the background region being of the same size several arcseconds away. The data were appropriately filtered and spectra obtained using version 14 of the XMM-SAS software, following standard data

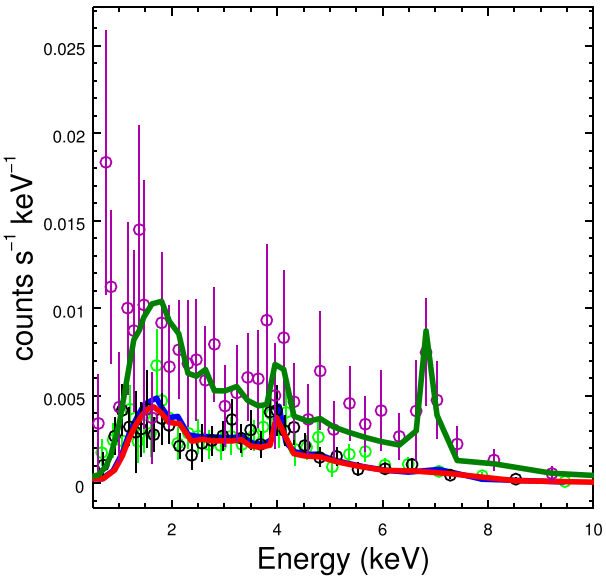

Figure 1. *XMM–Newton* MOS1, MOS2 and PN data and fits. All data sets were fitted simultaneously using the same thermal *vmekal* model, and required abundances of Ca, Ar and Fe in excess of solar values. MOS1 data are in light green, and the corresponding fit in blue. MOS2 data are in black, and the fit in red. The PN data are in purple with the fit in dark green. The similarity in the fits demonstrates that the same model adequately fits all data sets simultaneously. The Fe-K α line at 6.7 keV is visible in the PN data alone, a result of the effective area differences between the MOS and PN detectors at 6.7 keV.

reduction procedures. The *Chandra* SHERPA software (Freeman, Doe & Siemiginowska 2001) was used for analysis and fitting of all spectra. All the three data sets were fitted simultaneously to ensure the tightest constraints. Fig. 1 shows the spectra from the MOS1, MOS2 and PN instruments on board *XMM*, together with a thermal *vmekal* model that was used to jointly fit the three spectra. A Ca line at 4 keV can be seen. The presence of lines indicated that a thermal model was appropriate. In the fits, we find that allowing Ca, Ar, and Fe to deviate from solar values allows for the best fit. These elements were allowed to float freely but linked to have the same values in the MOS spectra, with only the normalization varying freely in each case. As can be seen from Fig. 1, the best-fitting normalization is quite similar for MOS1 and MOS2. In general with all the fits, it is clear that allowing the α-element values to float freely tends to improve the fit. The best-fitting abundances in both the MOS and PN fits were found to be higher than solar, with Fe and Ar having enhanced values >10 (in terms of Anders & Grevesse 1989 solar values), and Ca showing even larger abundances but with an equally large 1σ variation: 280±279. The MOS fits did not change appreciably with S thawed, but the PN fit demanded values of S $>$ 10. The best-fitting temperature is high, beyond the measurable range of *XMM–Newton*. In each case, we have used a single temperature model, which seems to match the spectra well. The best-fitting column density is found to be $9.4\pm0.29 \times 10^{21}$ cm^{-2}, consistent with the trend seen earlier. Unabsorbed fluxes are listed in Table 1. The error on the flux was computed using the SHERPA *sample_flux* routine, which computes the flux (typically) 1000 times, taking the variations in the parameters into account, and then determines the average flux and 1σ error from the computed fluxes.

We also attempted to fit a two-temperature model to the *XMM–Newton* data, tying the abundance values of the two components together. The two-temperature model results in a very low second temperature component as it tries to mainly fit the low-temperature region, giving temperatures around 0.2 keV. It does not change the fit appreciably, but increases the unabsorbed flux considerably, because the high column density results in an unabsorbed flux at low temperatures that significantly exceeds the absorbed flux. We do not consider these models viable, and they do not improve the fit in the high-temperature region. It is possible that allowing the abundance values of each component to vary completely independent of the other may provide a better fit. This also significantly increases the parameter space and fitting time, however. Our main purpose in this paper is to get a reasonable fit in order to estimate the flux and luminosity from the SN, and calculate the light curves. We have found that the one-component fits are adequate for this purpose. The fluxes so obtained are consistent within the error bars with those listed in the *XMM–Newton* Serendipitous Source Catalogue, 3XMM-DR4, further validating our choice of model and fits. Finally, some of the assumptions inherent to our model, such as ionization equilibrium, are validated in Section 4.

2.2 *Swift*

SN 2005kd was observed several times between 2007 and 2012 with the *Swift* X-ray Telescope (XRT), which has a 23 arcmin×23 arcmin field of view, 18 arcsec FWHM PSF (although the 90 per cent encircled energy diameter is ≈43 arcsec with mild energy dependence), and provides spectra over the 0.3–8.0 keV band with a spectral resolution of ≈0.1–0.2 keV. Processed data were retrieved from the *Swift* archive. A 35 arcsec region was used to extract the data, with the background obtained from a larger annulus region of 35–100 arcsec. Analysis was performed using FTOOLS and custom software. We filtered for event grades 0–12 only, used the standard XRT response matrix, and generated a position-dependent ancillary response file using the FTOOL program XRTMKARF, which provides nominal vignetting and PSF aperture corrections. Spectra close enough in time were binned together to provide sufficient signal to noise, as listed in Table 1.

Fig. 2 shows images from four different epochs during which *Swift* data were obtained. The SN was detected in 2007 and 2008 with a significance $>6\sigma$. In 2012, it was detected again but the significance was low ($\approx3.3\sigma$), prompting us to request a follow-up *Chandra* observation. The *XMM–Newton* and *Chandra* spectra reveal that the spectrum is clearly thermal in origin. Consequently, for those epochs where the SN was detected, we fitted the spectra using a single *vmekal* model. We note that the flux obtained for the 2007 data set is almost identical to that obtained by Immler et al. (2007). Our error bars are larger, which is understandable given that we actually fit the spectrum, rather than assuming a priori a thermal plasma with a temperature kT = 10 keV, and a Galactic $N_{\rm H}$ of 1.5×10^{21} cm^{-2} (Dickey & Lockman 1990). The best-fitting temperature is high (17 ±7 keV). The column density is also higher than that used by Immler et al. (2007), but due to the higher temperature, tends not to have as much of an effect on the flux. We find that the column density in the 2007 data set is $4.0\pm2.8 \times 10^{21}$ (over twice the Galactic value).

The 2008 data set initially gives a very high value of the column density ($>4.0 \times 10^{22}$ cm^{-2}), which results in an extremely high value of the unabsorbed flux ($>10^{-12}$ erg s^{-1} cm^{-2}), using either statistic. This value seems quite out of place with the previously obtained values, suggesting a sudden increase in column density, whereas the general trend seems to be slowly decreasing. However, plotting the variation of the column density versus temperature in the background fitted model shows that the 1σ range of possible

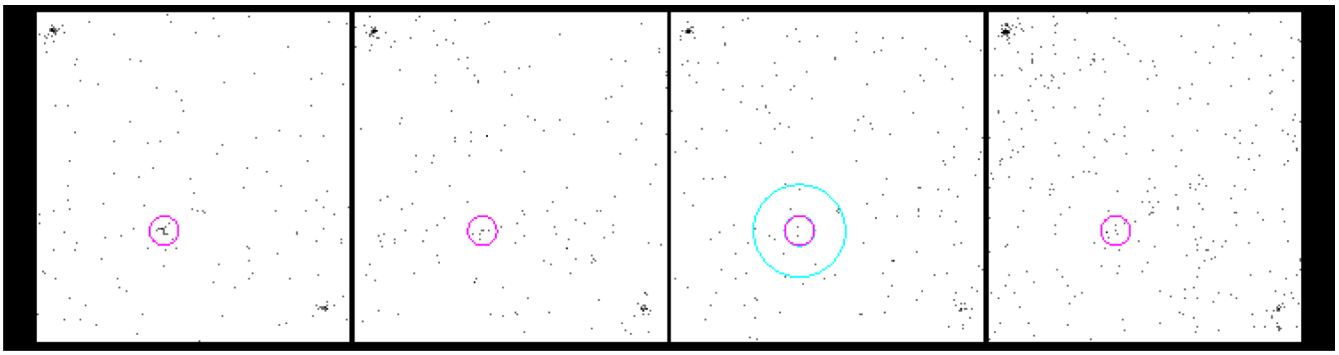

Figure 2. Images from the *Swift* observations of SN 2005kd, in the 0.3–8 keV energy range. From left to right: 2007, 2008, 2011 and 2012. The region is 11.5 arcmin on each side. The pink circle (35 arcsec in radius) denotes the region used to extract the data for SN 2005kd. The annulus used for the background region is shown in blue in the 2011 panel. Clearly, the SN is not detected in 2011, but it is detected in all the other frames.

values is large. By fixing the column to a much smaller value of 7.5×10^{21} cm^{-2} (intermediate between the two nearest values, but closer to the previous *Chandra* value), we find an almost equally good fit, with a flux that is an order of magnitude smaller. We have chosen to use this lower flux, which is more appropriate. We can reduce the column somewhat more, but the effect on the flux is within the error bars.

In 2011, the SN was not detected by *Swift* during an aggregate 9.3 ks XRT observation. Upper limits to the flux were calculated using the Bayesian method of Kraft, Burrows & Nousek (1991) for 99 per cent confidence. The uniform prior used by these authors results in fairly conservative upper limits, and other reasonable choices of priors do not materially change our scientific results. Within 35 arcsec, there are four counts, of which three are expected to be background based on a larger annulus region of 35–100 arcsec, once we scale by the source-to-background area difference. Using the Kraft et al. (1991) upper limits for this source + background, we derive a 99 per cent upper limit of 8.9 counts. With an exposure of 9.3 ks, this equates to 9.6×10^{-4} counts s^{-1}. Using the *Chandra* PIMMS calculator, we deduce an upper limit of 4.0×10^{-14} erg s^{-1} cm^{-2}. This upper limit is for the observed or absorbed flux. In order to get the unabsorbed flux, we used the *Chandra* PIMMS calculator, assuming an $N_{\rm H} = 4.0 \times 10^{21}$ cm^{-2} (again based on a decreasing $N_{\rm H}$ within the 2008 and 2012 values) and a temperature of 3.5 keV (intermediate between neighbouring values). A much lower temperature could increase the flux by about 30–40 per cent, but we think this is a better estimate given the parameters for the other observations closest in time. This gives an unabsorbed flux limit of about 6.7×10^{-14} erg s^{-1} cm^{-2}.

By 2012, the column density seems to have dropped to a value approaching the Galactic value, the temperature has decreased, and the flux is lower, as seen in Fig. 3.

2.3 *Chandra*

SN 2005kd was observed three times with the ACIS-S instrument on *Chandra*. Observations of 3 and 5 ks were made in 2007 (ObsID 8518) and 2008 (ObsID 9095), respectively. Even in these short observations, the SN was easily detected with $>13\sigma$ significance. After the SN was re-detected by *Swift* in 2012, we proposed for, and were awarded a 30 ks observation, which was carried out in 2013 November (ObsID 15999). The SN is detected with $>7\sigma$ significance, thus confirming the *Swift* re-detection.

The *Chandra* data were reduced and analysed using the analysis pipeline in the CIAO software version 4.7, and CALDB 4.6.8. A 4-arcsec

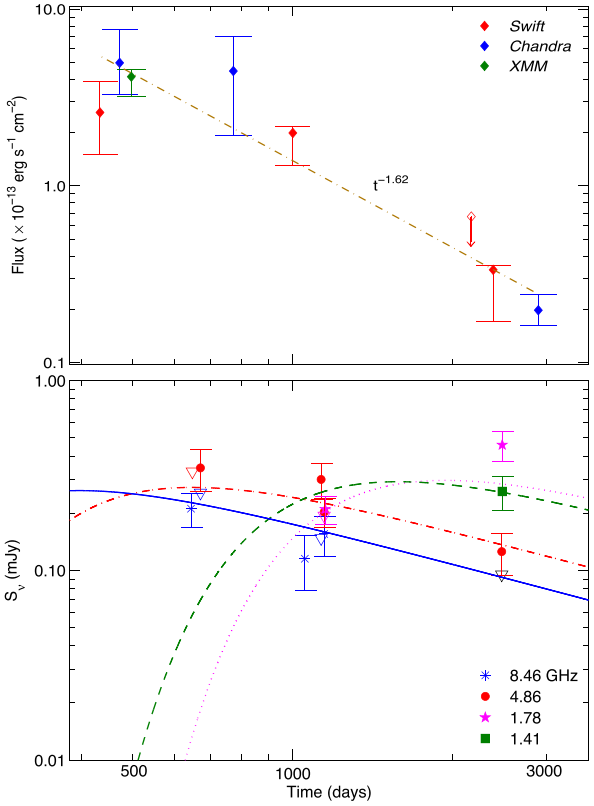

Figure 3. (Top) The 0.3–8 keV X-ray light curve of SN 2005kd (epochs listed in Table 1), showing unabsorbed flux with 1σ error bars. The time is given in the rest frame of the SN, along with the *k*-corrected flux. The data comprise of four *Swift*, three *Chandra* and one *XMM–Newton* data points. The best fit to the data is shown as a dashed line. It suggests the flux is decreasing as $t^{-1.62\pm0.06}$. (Bottom) Radio light curve of SN 2005kd at 8.46 GHz (blue, solid line), 4.86 GHz (red, dash–dotted line), 1.78 GHz (green, dashed line) and 1.41 GHz (magenta, dotted line). Downward triangles represent 3σ upper limits at the respective frequencies according to their colour. The black triangle is the upper limit at 7.91 GHz. The error bars represent $\pm1\sigma$. Where necessary, the flux has been converted to the appropriate frequency using the calculated radio spectral index. Fits to the data are shown and described further in Section 5. The few available data points do not allow for a robust fit, but the extracted parameter values are not inconsistent with those obtained from the X-ray data.

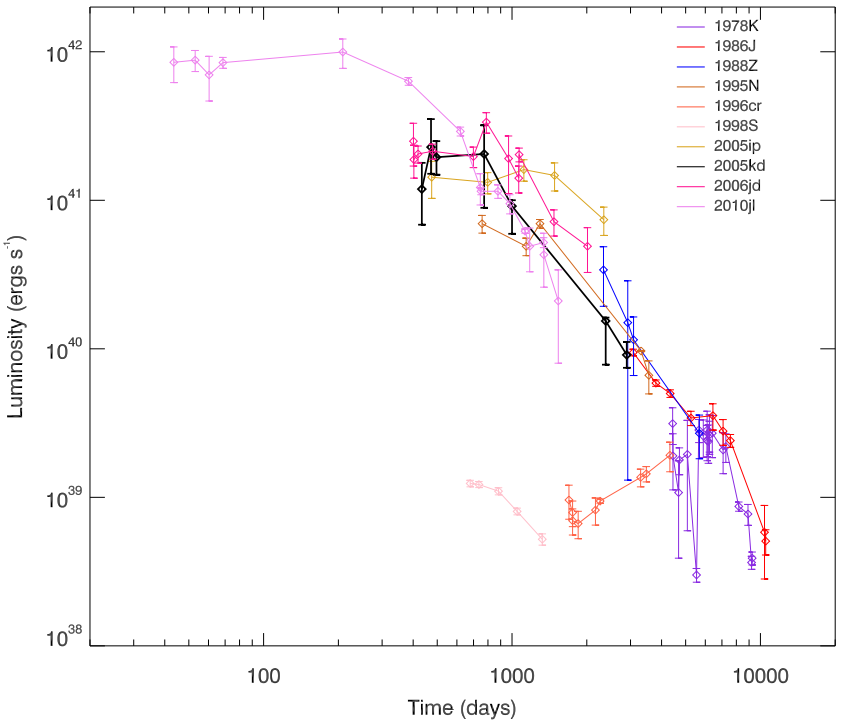

Figure 4. The light curves of observed Type IIn X-ray SNe that have multiple exposures. For information on the data for each SN, the X-ray fluxes, and the bands referenced for each SN, refer to Dwarkadas & Gruszko (2012), from which this figure has been adapted, with several additions. SN 2005kd is shown with a thick black line. Its X-ray luminosity is high even among IIn SNe, which in general have the highest luminosities of all X-ray-detected SNe.

source region centred on the point source was used. Our spectra were fitted with a thermal plasma *vmekal* model with a variable temperature and column density. Given the results from the *XMM–Newton* fitting, we thawed elements Ca and Fe, as well as Si. The C-statistic decreases, and the fit improves, when these elements are thawed. We find abundance values of Fe and Ca similar to those obtained with *XMM–Newton*, with Ca once again resulting in highly elevated abundance values with large error bars. For ObsID 8518, this gives a flux that is larger than the 2007 *Swift* value by almost 80 per cent. We note that Pooley et al. (2007) fitted a power-law model to the data, found a column density comparable to the Galactic one and a luminosity about 85 per cent higher than their *Swift* value, so these results are quite consistent. Our best fit gives a column density $7.7\pm1.7 \times 10^{21}$ cm^{-2}, which is higher than the Galactic column density. The best fit also suggests that the abundance of metals such as Fe and Ca exceeds the solar value.

SN 2005kd was observed again by *Chandra* 10 months later. The same thermal model was used as for the prior *Chandra* data set. We find the column density is $9.5\pm4.9 \times 10^{21}$ cm^{-2}, an elevated Ca abundance exceeding solar, and temperature of ~ 6 keV.

Finally, SN 2005kd was observed using ACIS-S on *Chandra* in 2013 November. As mentioned before, the SN was detected with a high significance, confirming its reappearance since 2011. The best-fitting thermal model gives a kT $= 1.47\pm0.39$ keV, and $N_{\rm H}$=$4.3 \pm1.11 \times 10^{21}$ cm^{-2}, with a preference for an elevated Si abundance. The column density is somewhat higher than the *Swift* 2012 value. The temperature is slowly decreasing as expected, since the higher temperatures in the first 500 d.

3 X-RAY LIGHT CURVE

Fig. 3 (top panel) shows the complete X-ray light curve of SN 2005kd calculated using background fitting. The data are converted to the rest-frame epoch, and *k*-corrected unabsorbed flux is plotted. The fluxes are calculated as indicated above, with 1σ error bars. Subsequent to the 2008 *Swift* observation, for over a 1000 d, there were no X-ray observations of SN 2005kd. We have combined exposures from 2011 October to 2012 January to get a combined almost 10 ks exposure with *Swift*. The SN is not detected at all within this exposure. However, it is in the next two exposures, with *Swift* and *Chandra*.

SN 2005kd represents one of the most X-ray luminous Type IIns. Fig. 4 shows the light curve of other observed Type IIn SNe. The X-ray light curve of SN 2005kd is shown as a thick black line. The upper limit from the *Swift* 2011 observation is not shown. It is clear that SN 2005kd is one of the most luminous, even among Type IIn SNe, with a luminosity exceeding 10^{40} ergs s^{-1} over a period of about 550 d starting from day 440. The total energy deposition, in the 0.3–8 keV X-ray band alone, from days 400 to about 3000 is $>10^{49}$ erg. The total energy in X-rays is likely to be much larger given the high temperatures inferred from spectral modelling. This means that the SN radiated more than 1 per cent of its kinetic energy within the first 3000 d at X-ray wavelengths, unless the kinetic energy substantially exceeds 10^{51} erg. Tsvetkov (2008) had calculated a lower limit to the energy radiated at optical wavelengths, finding it to be 3.2×10^{50} erg in the first 500 d. Either the SN is radiating away a large fraction of its energy in its first decade, or the total kinetic energy exceeds the canonical 10^{51} erg by a substantial margin.

4 ANALYSIS AND INTERPRETATION

The overall light curve of SN 2005kd from 440 to 3000 d indicates a decreasing luminosity with time. If we assume, as is generally the case, that the light curve decays as a power law in time, the best fit to the data points gives a light curve that decreases as $t^{-1.62\pm0.06}$

(Fig. 3). The temperature suggested by the first four epochs is higher than the range of values that can be measured by *Chandra*, *XMM–Newton* and *Swift*, and is thus relatively unconstrained. The column density is higher than the Galactic $N_{\rm H}$ towards that direction (1.5×10^{21} cm^{-2}) by a factor of 3–10, and appears to slowly decrease over time within the (large) error bars. At ∼1000 d, the best-fitting spectral model suggests a lower temperature and higher column density, but plotting the 2D confidence contours of temperature versus column density indicates that it is also compatible with the previous observations of a high temperature and $N_{\rm H}$ around five times the Galactic value.

The time evolution of the luminosity can be related to the density structure of the surrounding medium, as shown in Fransson, Lundqvist & Chevalier (1996) and Dwarkadas & Gruszko (2012). To summarize, if we use the Chevalier (1982) description for a SN shock wave evolving in a self-similar manner, assuming spherical symmetry, the SN ejecta has a density that goes as $\rho_{\rm SN} \propto v^{-n} t^{-3}$, and the uniform circumstellar medium (CSM) into which the SN evolves has a density profile that decreases as $\rho_{\rm CSM} \propto r^{-s}$, then the X-ray luminosity of the SN will decrease as

$$L_x \propto t^{-(12-7s+2ns-3n)/(n-s)}, \quad (1)$$

or

$$L_x \propto t^{-(6-5s+2ns-3n)/(n-s)} \qquad E << kT_{\rm sh}. \quad (2)$$

Equation (1) is valid when one is considering the total X-ray emission, equation (2) when one is considering the emission in an energy band E, where $E << kT_{\rm sh}$, and $T_{\rm sh}$ is the shock temperature. Neither is an exact fit to this situation; the latter is probably a better approximation over the first several hundred days, the former over the later period, but the resulting values are not significantly different using either equation. If we consider a luminosity decreasing as $t^{-1.62\pm0.06}$, we find that s varies between 2.3 and 2.46 for $n = 9$–12. Given the variation in parameters, we assume $s = 2.4\pm0.1$ in our analysis. This range of s indicates that the density decreases marginally faster than r^{-2}, which would be the case for a wind with constant mass-loss rate and wind velocity. We note from Fig. 4 that this steeper decrease is not uncharacteristic of Type IIn SNe at this age; in fact, many IIns appear to show a similar steep decrease in the light curves.

In order to calculate the mass-loss rate, we follow the procedure outlined in Fransson et al. (1996). Given the high temperature of the emission over most of the first 1000 d, we assume that it arises from the forward shocked CSM, and we do not see any emission from the reverse-shocked ejecta (this is addressed later). We will calculate the quantity $(\dot{M}/v_{\rm w})$ at a specific reference radius, 10^{15} cm. We use the *XMM–Newton* observation, given it has the best statistics. Following Fransson et al. (1996), we use the spectral luminosity at 1 keV. Since it is a spectral luminosity at a specific temperature, it is not modified by line emission, unless the line emission is present exactly at this frequency, which is not the case. We write the luminosity of the forward (circum-stellar) shock as $L_{\rm cs} \sim j_{\rm ff}(T_{\rm cs}) M_{\rm cs} \rho_{\rm cs}/m_{\rm H}^2$, where $j_{\rm ff}\, \rho_{\rm cs}/m_{\rm H}^2$ is the emissivity per unit mass, $\rho_{\rm cs}$ is the density behind the forward shock, $M_{\rm cs}$ is the mass swept-up by the forward shock, and $T_{\rm cs}$ is the temperature behind the forward shock. The Gaunt factor $g_{\rm ff}$ at 1 keV can be written as $g_{\rm ff} = 1.87\, T_8^{0.264}$, where T_8 is the forward shock temperature, $T_{\rm cs}$, in terms of 10^8 K. This approximation does not deviate by more than 30 per cent from more accurately tabulated values at each temperature, as long as the energy $E < 15$ keV, but may not be as appropriate for higher energies (Margon 1973). Using this value of $g_{\rm ff}$, we can write the luminosity of the forward shock at 1 keV as

$$L_{\rm cs,\,1\,keV} = 1.4 \times 10^{38}\, \xi\, T_8^{-0.236} \frac{e^{-0.116/T_8}}{(3-s)} \left[\frac{\dot{M}_{-5}}{v_{\rm w1}}\right]^2 \times V_4^{3-2s} \left[\frac{t_{\rm d}}{11.57}\right]^{3-2s} {\rm erg\,s^{-1}\,keV^{-1}}. \quad (3)$$

where $\dot{M}_{-5}$ is the mass-loss rate scaled to $10^{-5}{\rm M}_\odot$ yr^{-1}, $v_{\rm w1}$ is the wind velocity in terms of 10 km s^{-1}, V_4 is the maximum ejecta velocity scaled to 10^4 km s^{-1}, $\xi = [1 + 2n(He)/n(H)]/[1 + 4n(He)/n(H)] \sim 0.85$, and $t_{\rm d}$ is the time in days. We note that this expression has different approximations from the previous ones, and is independent of n. For $s = 2.4$, it gives a flux decreasing as $t^{-1.8}$. It is close enough given the other uncertainties.

At 500 d, the average *XMM* flux at 1 keV is $6.53^{+2.13}_{-1.73} \times 10^{-14}$ erg s^{-1} cm^{-2} keV^{-1}. Using a distance of 63.2 Mpc, and inserting in equation (3), with values of $0.6 < V_4 < 0.9$, $6 \le T_8 \le 9$, and $2.3 < s < 2.5$ in equation (3) gives

$$192 \le \left[\frac{\dot{M}_{-5}}{v_{\rm w1}}\right] \le 656. \quad (4)$$

Therefore, we deduce that, for a wind velocity of 10 km s^{-1}, the mass-loss rate must be around $(1.9–6.6) \times 10^{-3}{\rm M}_\odot$ yr^{-1} at 10^{15} cm. If the wind velocity is higher, the mass-loss rate is correspondingly higher. It is difficult to find a progenitor that satisfies the velocity, mass-loss rate and light-curve characteristics (discussed in further detail in Section 6). We emphasize that the mass-loss rate is a time-varying quantity. However, it is clear that the ambient medium around the SN has a high density.

As described in Section 2, we have assumed thermal models to describe the SN, which are in ionization equilibrium. We can now go back and confirm if that approximation is reasonable. We note that we have calculated the mass-loss rate and wind velocity at 10^{15} cm; thus, the electron density at 10^{15} cm is

$$n_e = \left[\frac{1}{4\pi \times 10^{30}\, \xi m_{\rm H}}\right]\left[\frac{\dot{M}}{v_{\rm w}}\right] \sim (6.8 - 23) \times 10^9 \ \ {\rm cm^{-3}} \quad (5)$$

where $m_{\rm H}$ is the mass of a hydrogen atom. At any given radius, the density is $(6.8–23) \times 10^9 (r_0/r)^s$ cm^{-3}, where $r_0 = 10^{15}$ cm. We assume that for ionization equilibrium, the condition is that $n_e t \sim 10^{12}$ cm^{-3} s (Smith & Hughes 2010).

At 500 d, assuming an average shock velocity of 6000–9000 km s^{-1} (appropriate for the high density), the shock radius is $2.6–3.9 \times 10^{16}$ cm. We have $n_e t|_{500\,\rm d} \sim (0.45–4) \times 10^{14}$ cm^{-3} s for $s = 2.4$. At 1000 d, assuming a slightly slower average velocity of 5000–8000 km s^{-1}, the shock radius is $4.32–6.9 \times 10^{16}$ cm, and the corresponding value is $(2.26–23.6) \times 10^{13}$ cm^{-3} s for $s = 2.4$. For $s = 2.5$, the density is somewhat lower, but still gives values $>10^{12}$ cm^{-3} s, whereas for $s = 2.3$, the density is higher. In all cases, we may conclude that the plasma is in ionization equilibrium at all times during which the observations were taken. A lower velocity will give a smaller radius and higher density so it will further reinforce this argument. Thus, we can justify our use of models for plasma in ionization equilibrium.

Why do we not see (low-temperature) emission from the reverse shock, given that the temperature behind this shock is lower, and more likely to fall in the range of *Swift*, *XMM–Newton* and *Chandra*? Presumably, it is because most of the emission from the reverse shock is absorbed. This is possible if the reverse shock is radiative and a cool dense shell has formed behind it, which absorbs the emission from the shock. The cooling time from the reverse shock

can be written as

$$t_{\rm cool,r} = 3.5 \times 10^9 \frac{(4-s)(3-s)^{4.34}}{(n-3)(n-4)(n-s)^{3.34}} \times V_4^{3.34+s} \left[\frac{\dot{M}_{-5}}{v_{\rm w1}}\right]^{-1} \left[\frac{t_{\rm d}}{11.57}\right]^{s} s. \quad (6)$$

For $2.3 < s < 2.5$, $9 < n < 12$, and $V_4 < 1$, we find that the reverse shock is radiative throughout the evolution, for the derived values of $\left[\frac{\dot{M}_{-5}}{v_{\rm w1}}\right]$. Thus, our initial assumption of the emission arising from the forward shock is validated. For large values of n, the cooling time goes as $n^{-5.34}$ and thus is strongly dependent on the value of n. The shock will be radiative for any larger value of n.

Within the error bars, we find that the column density is 3–10 $\times$ 10^{21} cm^{-2}, and decreases slowly over the first 1000 d. This suggests that there is some extra absorbing column density ahead of the forward shock too. Assuming the ambient density extends outwards continually with the same slope, the column density ahead of the circum-stellar shock can be written as

$$N(H)_{\rm cs} = 2.1 \times 10^{22} \left[\frac{\dot{M}_{-5}}{(s-1)\, v_{\rm w1}}\right] V_4^{1-s} \left[\frac{t_{\rm d}}{8.9}\right]^{1-s} {\rm cm}^{-2}. \quad (7)$$

We note that this is the additional column that must be added to the value of the Galactic column density. For parameters between $\left[\frac{\dot{M}_{-5}}{v_{\rm w1}}\right] \sim 192{-}656$, $0.6 < V_4 < 0.9$, $s = 2.3$–2.5 and $t_{\rm d} < 1000$, this value starts off as a few to several times larger than the measured column of $\sim$3–10 $\times$ 10^{21}, and then slowly decreases, with the decrease being larger for higher values of s as expected from equation (7). For values of $s = 2.4$–2.5 and the lower end of the mass-loss rate, the column density is generally less than the Galactic column by about 3000 d, and does not contribute much. For $s = 2.3$, the value is still larger than Galactic even at day 3000. For the top end of the mass-loss rate range, the values are quite high, especially for $s = 2.3$ and low V_4. The highest mass-loss rates are less likely, since we do not see such a large observed column, unless the medium is almost fully ionized (which is not the case as we show below). This implies that higher values of s, combined with mass-loss rates at the lower end of their appropriate range for high$s$, are more probable.

The time-scale for recombination is $\sim 3 \times 10^{12}/n_e$ s. Using n_e from equation (5), we see that the circum-stellar material ionized by the progenitor star would have already recombined by the time the shock wave reaches it (see also Dwarkadas 2014). Hence, the main mechanism for ionization of the medium is the X-ray emission itself, which depends on the ionization parameter $\chi = L/nr^2$ (Kallman & McCray 1982). This can be written as

$$\chi = 2 \times 10^{-38}\, L\, \xi^{-2} \left[\frac{\dot{M}_{-5}}{v_{\rm w1}}\right]^{-1} V_4^{s-2} \left[\frac{t_{\rm d}}{8.9}\right]^{s-2}. \quad (8)$$

Note that for $s = 2$, this becomes independent of time (if L is not time-dependent), as expected. For the luminosities of 2005kd, and the high densities, the value of χ should be less than 100 throughout most if not all of the evolution. For high temperatures outside the range probed by *Chandra* and *XMM–Newton*, e.g. $T_8 \sim 10$, Chevalier & Irwin (2012) find that elements such as C, N, and O are only ionized when $\chi \sim 500$. This indicates that even the elements like C, N, and O are not fully ionized in the high-temperature plasma. Heavier elements such as Fe are only ionized at $\chi \sim 5000$ (Chevalier & Irwin 2012). Overall, the ionization factor is very low, which suggests that the medium is mainly neutral, and we are seeing almost the entire column that is present. The combination of equations (7) and (8) indicates a preference for higher values of s, which give higher ionization parameter and lower column, that is more consistent with the data.

5 RADIO EMISSION FROM 2005kd

In an attempt to further constrain the evolution, we have investigated the radio emission from the SN. We have analysed SN 2005kd radio data at three different bands obtained with the Very Large Array (VLA). Data reduction was done following standard procedures using the NRAO Astronomical Image Processing System (AIPS) for data taken in 2009 and earlier. For data taken after the VLA upgrade completion, we used the Common Astronomy Software Applications package (CASA; McMullin et al. 2007).

We used natural weighting in the imaging process of all the epochs to increase their sensitivity. Additionally, there were observations at 22 GHz made in 2005 November and 2007 August, but no detections were obtained. We do not discuss the emission at this frequency further since the limits provide no additional constraints.

The observations included here were made using 0410+769 as a phase calibrator. To test the reliability of the SN flux density variations, we made maps of the phase calibrator and measured a peak intensity of $\sim$2.7 Jy beam^{-1} for all the 4.5 GHz observations, and $\sim$1.8 Jy beam^{-1} at 8.5 GHz. At 4.5 GHz, there is also a visible source at about 1.2 arcmin west from SN 2005kd. This source has a flux density $\sim$1 mJy beam^{-1} in all those epochs. Thus, we consider the flux densities shown in Table 2 as highly robust measurements. The upper limits are given at a 3σ confidence level.

The SN was detected as a point source, hence, the peak intensities shown in Table 2 also represent flux densities. The uncertainties include the contribution of the local rms and a conservative uncertainty in the absolute flux calibration of 5 per cent. We note that the 2007 August 14 epoch corresponds to the radio discovery reported by Chandra & Soderberg (2007). Their value and the one we report here are consistent within the uncertainties. Furthermore, the epochs previous to the VLA upgrade in 2009 are limited by a poor dynamic range owing to the existence of other sources in the field which are much stronger than the SN itself. To account for this effect, we have carefully measured any background emission at the position of the SN in each epoch.

SN 2005kd was detected in the L, C and X bands over the first 9 yr. The C- and X-band flux densities are decreasing with time, whereas the L-band light curve appears to be still rising. Thus, the radio emission appears to have already peaked at the higher frequencies and transitioned from the optically thick to the optically thin regime at 4.86 and 8.46 GHz, whereas it is perhaps still in the optically thick phase, or just transitioning to the optically thin phase at 1.4 GHz. This is consistent with observations of other radio SNe (Weiler et al. 2002). On 2012 August, the two-point spectral index between 4.49 and 1.78 GHz is $\alpha = -0.72 \pm 0.35$. Using this information, and assuming that the flux varied little between August 16 and 22, and that the spectral index extends from 1.78 to 4.86 GHz, we have converted the flux density measured on 2012 August 16 at 4.49 GHz to a flux at 4.86 GHz. The corresponding value is $125.37 \pm 31.35\mu$Jy beam^{-1}.

We have fitted (see Fig. 3) a multifrequency light curve to the data shown in Table 2, following the parametrization described in Weiler et al. (2002), using a Monte Carlo simulation to obtain a robust fit (see details in Romero-Cañizales et al. 2014). We have adopted $\alpha = -0.72$ and t_0 =2005-Nov-10 as explosion date (Tsvetkov 2008). The optically thick region is generally attributed to absorption by the external medium or the medium internal to the SN (free–free absorption, FFA) or due to synchrotron self-absorption

Table 2. VLA observations of SN 2005kd.

Observation date	Days after outburst (rest frame)	ν (GHz)	Conv. beam (arcsec^2)	rms (μJy beam^{-1})	Peak intensity (μJy beam^{-1})
2007-August-14	632.5	8.46	0.38×0.29, −42.°7	42.42	211.06±43.71
2007-September-10	659.1	8.46	0.37×0.29, 40.°3	80.19	<255.85
2008-September-27	1036.4	8.46	0.37×0.26, −35.°9	36.24	115.09±36.69
2008-December-13	1112.3	8.46	0.39×0.24, −36.°5	47.88	<147.47
2008-December-28	1127.1	8.46	0.36×0.24, −20.°4	36.37	155.36±37.19
2012-August-16	2434.4	7.91	1.47×0.89, −2.°2	31.10	<94.92
2007-August-18	636.4	4.86	0.62×0.44, −37.°6	82.41	<331.13
2007-September-10	659.1	4.86	0.58×0.44, 38.°2	85.56	346.57±87.30
2008-December-13	1112.3	4.86	0.93×0.38, −42.°3	64.04	300.91±65.78
2008-December-28	1127.1	4.86	0.74×0.36, −33.°0	33.56	202.54±35.05
2012-August-16	2434.4	4.49	2.57×1.57, −2.°0	32.53	132.80±33.20
2008-December-28	1127.1	1.42	2.66×1.41, −45.°3	47.71	<193.57
2009-January-02	1132.0	1.42	2.52×1.37, −6.°7	34.54	209.94±36.10
2012-August-22	2440.3	1.41	6.71×5.18, −178.°2	79.14	458.04±82.39
2012-August-22	2440.3	1.78	5.32×4.08, 1.°1	51.70	269.40±53.31

(SSA). SN 2005kd displayed radio emission at late stages in its evolution, and a high but non-relativistic ejecta velocity (based on the X-ray temperatures in the first 1000 d). Hence, we exclude the contribution of a clumpy CSM (see e.g. van Dyk et al. 1994), as well as SSA (Chandra et al. 2012; Romero-Cañizales et al. 2014) and consider FFA in the uniform local CSM. Thus, to represent the flux density evolution at a given frequency, we have used

$$\left(\frac{S}{1\,\mathrm{mJy}}\right) = K_1 \left(\frac{\nu}{5\,\mathrm{GHz}}\right)^{\alpha} \left(\frac{t-t_0}{1\,\mathrm{d}}\right)^{\beta} e^{-\tau_{\mathrm{CSM}}} \quad (9)$$

where

$$\tau_{\mathrm{CSM}} = K_2 \left(\frac{\nu}{5\,\mathrm{GHz}}\right)^{-2.1} \left(\frac{t-t_0}{1\,\mathrm{d}}\right)^{\delta}.$$

The fitted parameters ($K_1 = 13.5$–148.0, $K_2 = 2.4 \times 10^4$–7.4×10^7, $\beta = -0.74^{+0.16}_{-0.17}$ and $\delta = -2.36^{+0.46}_{-0.66}$) allow us to infer a peak luminosity at 4.86 GHz of 1.29×10^{27} erg s^{-1} on day 631 after explosion (rest frame). We thus estimate a mass-loss rate of $\sim 0.5 \times 10^{-4}\,\mathrm{M}_{\odot}$ yr^{-1} (assuming a wind velocity of 10 km s^{-1} and using equation (17) from Weiler et al. 2002) at a radius of $\sim 4.6 \times 10^{16}$ cm. The fit gives a value $s = 1.82 \pm 0.37$. This slope is a bit lower than our X-ray-derived values. It is clear that there are problems with both the fit and its interpretation. The former is due to the sparsity of data, which makes fitting unreliable; the latter is mainly due to the complexity of the system.

The smooth decline of the radio emission at both 4.86 and 8.46 GHz suggests a fairly smooth transition from 1000 to 3600 d. However, the long-lasting radio emission does favour the presence of an overall high-density CSM, which is also inferred from the X-rays.

6 DISCUSSION AND CONCLUSIONS

In the previous section, we form an overall picture of Type IIn SN 2005kd. In our model, the SN expands in a medium with a density slope $s \sim 2.3$–2.5, with a value of $\left[\frac{\dot{M}_{-5}}{v_{w1}}\right] \sim 192$–$656$ at a radius of 10^{15} cm, and decreasing with time. The X-ray emission is likely dominated by the forward shock, with a high temperature and a column density that reflects the high mass-loss rate. The reverse shock remains radiative, with all emission from the reverse shock being absorbed by a presumed cool dense shell behind it. The data suggest a slight, although not conclusive, preference for higher values of $s = 2.4$–2.5, and lower mass-loss rates. Further observations are needed to confirm or refute this.

This analysis of the X-ray emission from a Type IIn SN confirms that the SN expands into a very high-density medium with density decreasing somewhat faster than r^{-2}. The density is higher than those encountered around the majority of stars. This is consistent with other Type IIns, although as we see from Fig. 4, SN 2005kd's X-ray luminosity appears to exceed that of most Type IIn SN. The instantaneous density at any given radius, $\dot{M}_{\mathrm{r}}$, can be written as: $\dot{M}_{\mathrm{r}} \propto \dot{M}(r/r_0)^{2-s}$. For $s = 2.4$ $\dot{M}_{\mathrm{r}} \propto (r/r_0)^{-0.4}$. Thus, the mass-loss rate at 4.0×10^{16} cm would be about 77 per cent lower than that at 10^{15} cm. Note that this indicates that the mass-loss rate was likely higher than $10^{-4}\mathrm{M}_{\odot}$ yr^{-1} at 4.0×10^{16} cm.

The density profile is likely somewhat steeper than an r^{-2} density profile, indicating a variation in the wind parameters in the years leading up to the SN explosion. If we assume that the wind velocity was of the order of 10 km s^{-1}, then this variation occurred over at least the last 5000–7000 yr of stellar evolution, suggesting that the progenitor star increased its mass-loss rate (and/or decreased the wind velocity) a few thousand years before explosion.

It is hard to determine which progenitor best fits this analysis. The high mass-loss rate of 0.43–$1.5 \times 10^{-3}\mathrm{M}_{\odot}$ yr^{-1}, at 4.0×10^{16} cm, for a 10 km s^{-1} wind, is too high even for an RSG star at the extreme high-mass end of mass-loss rates (Mauron & Josselin 2011). Humphreys et al. (1997) have shown that the yellow hypergiant IRC+10420 may have undergone high mass-loss episodes where it lost mass at a rate of $10^{-3}\mathrm{M}_{\odot}$ yr^{-1} for about a 1000 yr. This is lower than the time period of high mass-loss inferred by us for a wind velocity of $\sim$10 km s^{-1}, but not significantly so. It is possible that a hypergiant star with a somewhat higher mass-loss rate may just about meet the required characteristics at the lower end of the deduced mass-loss rate. The star must lose several solar masses of material in this period. The derived high Ca abundances are consistent with the finding that supergiant atmospheres are rich in Ca-Al silicates (Speck et al. 2000). An RSG or hypergiant progenitor is also compatible with the fact that the optical light curve from 2005kd showed a plateau for about 192 d (Tsvetkov 2008), indicating that it may arise from a progenitor with a large stellar radius. In this context, it is interesting to note that, from an analysis of their *R*-band light, it has been found that the SNe IIn population statistically bears more similarity to the SN IIP population than the SN Ic population (Habergham et al. 2014). The latter would be

expected for really massive progenitors. The overall behaviour of SN 2005kd is reminiscent of other IIns that show photometric evolution similar to IIPs. Mauerhan et al. (2013) have defined a subclass of SNe called Type IIn-P to describe these SNe that showed both IIn and IIP characteristics. The energy radiated by all of these in the plateau phase must arise from CSM interaction, as demonstrated for SN 2005kd. As compared to the IIn-Ps, however, SN 2005kd shows a much longer plateau duration, and does not appear to decline as rapidly as the others at the end of the plateau phase. Unfortunately, the lack of optical spectroscopy on SN 2005kd precludes more detailed comparison.

If the surrounding wind velocity were assumed to be much higher than 10 km s^{-1}, the mass-loss rate would need to be correspondingly higher, thus making it difficult to ascribe a known progenitor to the SN. LBVs have been suggested as IIn progenitors. Their wind velocities are about an order of magnitude higher than those of RSGs, and consequently, the required mass-loss rates would jump up by an order of magnitude. LBVs undergoing a giant eruption (Smith 2014) would be needed to satisfy the required mass-loss rates, which would exceed $1 \times 10^{-3} M_{\odot}$ yr^{-1} for LBV wind velocities at 4.0×10^{16} cm. The high mass-loss rates would also have to be sustained for several hundred years, which has generally not been observed in LBVs. Importantly, any progenitor without a large stellar radius as in RSGs would furthermore require a different explanation for the plateau region in the optical light curve. This could perhaps be a consequence of the SN being surrounded by a massive dense shell into which the shock expanded after breakout (Dessart et al. 2016). The shell would have to exist from a radius of around 10^{16} cm, given the current observations.

We have interpreted the obvious high density suggested by the observations as a high mass-loss rate (in equation 3). This, however, is not the only interpretation. A high-density shell can also be due to sweeping up of external material by a lower density wind (Dwarkadas 2011). A similar model was found adequate to explain the X-ray emission from SN 1996cr (Dwarkadas et al. 2010). The decreasing light curve makes this appear less likely in the present case, however, the lack of X-ray observations in the first 400 d makes it difficult to entirely rule out the possibility.

Fig. 4 shows the similarity between the X-ray evolution of SN 2006jd and that of SN 2005kd. The X-ray luminosities are comparable. Chandra et al. (2012), in their interpretation of the X-ray light curve from SN 2006jd, have approximated it as a simple power-law decline, similar to our assumption here. Their derived densities were in excess of 10^6 cm^{-3} at 1000 d, comparable to the values found herein. The slope that they found was less steep than that found here, but overall, the similarities between these two Type IIns are obvious.

In summary, SN2005kd provides further confirmation that IIn SNe evolve in high mass-loss rate winds (Ofek et al. 2007; Smith et al. 2007; Chatzopoulos et al. 2011; Chandra et al. 2012; Fransson et al. 2014). They often appear to show rapid changes in wind parameters near the end of the star's lifetime. Such changes have also been postulated for many other Type IIn SNe (Dwarkadas et al. 2010, and references within). The high mass-loss rates could just about accommodate a hypergiant star as a progenitor. An alternative possibility is that the surrounding wind velocity, and consequently mass-loss rate, are higher, and the progenitor is not an RSG that turned hypergiant but an LBV star undergoing a giant eruption, as has been often suggested for IIns. The latter though would require extremely high mass-loss rates to be sustained for at least several hundred years. Any progenitor model must also be able to account for the change in wind parameters in the years prior to the explosion, as well as the optically observed plateau region. Further continual and consistent monitoring of Type IIn SNe at all wavelengths, but particularly in the X-ray and radio bands, is suggested if we are to unambiguously determine their progenitors.

ACKNOWLEDGEMENTS

We acknowledge the anonymous referee for diligently reading the paper, and providing extremely valuable comments that have considerably improved the manuscript. The scientific results reported in this paper are based on observations made by the *Chandra, Swift* and *XMM–Newton* X-ray observatories, and by the Very Large Array, NRAO Socorro, which is a facility of the National Science Foundation operated under cooperative agreement by Associated Universities, Inc. This research has made use of data obtained from the Chandra Data Archive and the HEASARC archive, and software provided by the Chandra X-ray Center (CXC) in the application packages CIAO, CHIPS, and SHERPA. We gratefully acknowledge support from grant GO4-15075X, provided by NASA through the Chandra X-ray Observatory center, operated by SAO under NASA contract NAS8-03060 (VVD, FEB); and from the NASA Astrophysics Data Analayis program grant NNX14AR63G awarded to University of Chicago (VVD). We also acknowledge support from CONICYT through FONDECYT grant 3150238 (CR-C) and from project IC120009 'Millennium Institute of Astrophysics' (MAS) funded by the Iniciativa Científica Milenio del Ministerio Economía, Fomento y Turismo de Chile (CR-C, FEB), from CONICYT-Chile grants Basal-CATA PFB-06/2007 (CR-C, FEB), FONDECYT 1141218 (FEB), PCCI 130074 (FEB), ALMA-CONICYT 31100004 (CR-C, FEB), and 'EMBIGGEN' Anillo ACT1101 (CR-C,FEB).

REFERENCES

Anders E., Grevesse N., 1989, Geochim. Cosmochim. Acta, 53, 197
Bauer F. E., Zelaya P., Clocchiatti A., Maund J., 2012, Proc. IAU Symp. 279, Death of Massive Stars: Supernovae and Gamma-Ray Bursts. Kluwer, Dordrecht, p. 325
Chandra P., Soderberg A., 2007, Astronomer's Telegram, 1182, 1
Chandra P. et al., 2009, ApJ, 690, 1839
Chandra P., Chevalier R. A., Chugai N., Fransson C., Irwin C. M., Soderberg A. M., Chakraborti S., Immler S., 2012, ApJ, 755, 110
Chatzopoulos E. et al., 2011, ApJ, 729, 143
Chevalier R. A., 1982, ApJ, 258, 790
Chevalier R. A., Irwin C. M., 2012, ApJ, 747, L17
Dessart L., Hillier D. J., Audit E., Livne E., Waldman R., 2016, MNRAS, 458, 2094
Dickey J. M., Lockman F. J., 1990, ARA&A, 28, 215
Dwarkadas V. V., 2011, MNRAS, 412, 1639
Dwarkadas V. V., 2014, MNRAS, 440, 1917
Dwarkadas V. V., Gruszko J., 2012, MNRAS, 419, 1515
Dwarkadas V. V., Dewey D., Bauer F., 2010, MNRAS, 407, 812
Eastman J. et al., 2005, Cent. Bur. Electron. Telegrams, 290, 1
Eldridge J. J., Fraser M., Smartt S. J., Maund J. R., Crockett R. M., 2013, MNRAS, 436, 774
Filippenko A. V., 1997, ARA&A, 35, 309
Fox O. D. et al., 2011, ApJ, 741, 7
Fox O. D., Filippenko A. V., Skrutskie M. F., Silverman J. M., Ganeshalingam M., Cenko S. B., Clubb K. I., 2013, AJ, 146, 2
Fransson C., Lundqvist P., Chevalier R. A., 1996, ApJ, 461, 993
Fransson C. et al., 2014, ApJ, 797, 118
Freeman P., Doe S., Siemiginowska A., 2001, in Starck J.-L., Murtagh F. D., eds, Proc. SPIE Conf. Ser. Vol. 4477, Astronomical Data Analysis. SPIE, Bellingham, p. 76

Gal-Yam A., Leonard D. C., 2009, Nature, 458, 865
Habergham S. M., Anderson J. P., James P. A., Lyman J. D., 2014, MNRAS, 441, 2230
Humphreys R. M. et al., 1997, AJ, 114, 2778
Immler S., Pooley D., Brown P. J., 2007, Astronomer's Telegram, 981, 1
Kallman T. R., McCray R., 1982, ApJS, 50, 263
Kankare E. et al., 2012, MNRAS, 424, 855
Kraft R. P., Burrows D. N., Nousek J. A., 1991, ApJ, 374, 344
McMullin J. P., Waters B., Schiebel D., Young W., Golap K., 2007, in Shaw R. A., Hill F., Bell D. J., eds, ASP Conf. Ser. Vol. 376, Astronomical Data Analysis Software and Systems XVI. Astron. Soc. Pac., San Francisco, p. 127
Margon B., 1973, ApJ, 184, 323
Mauerhan J. C. et al., 2013, MNRAS, 431, 2599
Mauron N., Josselin E., 2011, A&A, 526, A156
Ofek E. O. et al., 2007, ApJ, 659, L13
Pooley D., Immler S., Filippenko A. V., 2007, Astronomer's Telegram, 1023, 1
Pritchard T. A., Roming P. W. A., Brown P. J., Bayless A. J., Frey L. H., 2014, ApJ, 787, 157
Puckett T., Pelloni A., 2005, Cent. Bur. Electron. Telegrams, 285, 1
Romero-Cañizales C. et al., 2014, MNRAS, 440, 1067
Schlegel E. M., 1990, MNRAS, 244, 269
Smith N., 2010, in Leitherer C., Bennett P. D., Morris P. W., Van Loon J. T., eds, ASP Conf. Ser. Vol. 425, Hot and Cool: Bridging Gaps in Massive Star Evolution. Astron. Soc. Pac., San Francisco, p. 63
Smith N., 2014, ARA&A, 52, 487
Smith R. K., Hughes J. P., 2010, ApJ, 718, 583
Smith N. et al., 2007, ApJ, 666, 1116
Smith N., Hinkle K. H., Ryde N., 2009, AJ, 137, 3558
Speck A. K., Barlow M. J., Sylvester R. J., Hofmeister A. M., 2000, A&AS, 146, 437
Taddia F. et al., 2013, A&A, 555, A10
Tsvetkov D. Y., 2008, Perem. Zvezdy, 28, 6
van Dyk S. D., Weiler K. W., Sramek R. A., Rupen M. P., Panagia N., 1994, ApJ, 432, L115
Weiler K. W., Panagia N., Montes M. J., Sramek R. A., 2002, ARA&A, 40, 387

This paper has been typeset from a TEX/LATEX file prepared by the author.